Days to Decades: Forecasting Neutral Densities in Low Earth Orbit

Matthew K. Brown
SERENE, University of Birmingham, UK

Sean Elvidge, David R. Themens
SERENE, University of Birmingham, UK

Hugh G. Lewis
University of Southampton, UK

Andrew J. Kavanagh, Ingrid Cnossen
British Antarctic Survey, UK

ABSTRACT

The SWIMMR (Space Weather Instrumentation, Measurement, Modelling and Risk) programme is improving the UK's capability for space weather monitoring and prediction. The thermosphere part of the programme (SWIMMR-T) focuses on both short and long-term neutral density forecasting within Low Earth Orbit (LEO). For short-term forecasting up to 48 hours, the Advanced Ensemble electron density Assimilation System (AENeAS) is being made operational at the UK's Met Office Space Weather Operations Centre (MOSWOC), with neutral densities available to end users. These improved forecasts will aid operators with conjunction analysis and re-entry predictions through better understanding of the atmospheric drag perturbation on satellite orbits.

Assimilative atmospheric models fuse together global observations of the state of the atmosphere with a background model to provide a reduced error estimate of the current state. AENeAS is a 4D physics-based data assimilation model of the ionosphere-thermosphere system. It uses the Thermosphere Ionosphere Electrodynamics General Circulation Model (TIE-GCM) as the background numerical model, solving 3D momentum, energy and continuity equations to allow physics-based nowcasting and forecasting from an observation-constrained hindcast. However, TIE-GCM has an upper boundary of between 400 and 700 km, dependent upon solar activity conditions. Constituent profiles have been extrapolated above this using a Bates-Walker profile fitted to the modelled altitudes, allowing reconstruction of neutral densities throughout LEO regardless of solar activity levels.

Assimilation within AENeAS is performed via a local ensemble transform Kalman filter (LETKF). Previously total election content (TEC) and ground-based ionosonde observations were assimilated into AENeAS, with the ionosphere constraining the thermosphere. We now also assimilate neutral densities derived from the energy dissipation rates (EDR) between Orbit Mean-elements Messages (OMMs). OMMs are pre-processed through use of an extended Density-Based Scattering Clustering of Applications with Noise (DBSCAN) algorithm adapted to be used with objects across the LEO regime. This identifies manoeuvres and removes outliers to provide more accurate EDR-derived densities.

These neutral densities will be made available via the Met Office via gridded data, or tailored products upon request.

The SWIMMR-T project also identifies that long-term forecasts currently assume a fixed climatology. However, rising carbon dioxide concentrations are leading to global cooling in the upper atmosphere, causing thermospheric contraction and reducing neutral densities at fixed altitudes. Previous studies observed a trend of between 2 and 5 % reduction per decade in neutral densities at 400 km, with the lower value at higher solar activity levels. The Whole Atmosphere Community Climate Model with thermosphere and ionosphere extension (WACCM-X) has been used to quantify by how much the upper atmosphere contracts based on future ground-level carbon dioxide concentrations. The Representative Concentration Pathways (RCPs) published by the Intergovernmental Panel on Climate Change (IPCC) provide four scenarios for carbon dioxide concentration through to the year 2100. These can be used along with the WACCM-X results to provide neutral density "forecasts" through to 2100 which account for long-term climatological change. In turn, these can be used to investigate the long-term impacts on the debris environment. The Binned Representative Atmospheric Decay (BRAD) debris model has been used to model these impacts.

1. INTRODUCTION

Below around 600 km altitude, the two major orbital perturbations are Earth's oblateness (J2 specifically) and atmospheric drag [1]. While the effects of Earth's asymmetry are well quantified and constant, atmospheric drag varies on both short and long timescales by up to an order of magnitude. This is due to the thermosphere coincident with Low Earth Orbit (LEO) expanding and contracting primarily due to input solar energy, but also through its connection with the lower parts of the atmosphere [2, 3]. The complexity of the upper atmosphere system, along with a relative lack of direct observations, make it a difficult system to model. Empirical models such as NRLMSISE-00, are fit to the data of long-term climatologies and allow for fast simulation of the upper atmosphere [4]. However they are limited to the data used within their creation, and struggle to capture smaller-scale phenomena. Numerical models directly solve for the physics, chemistry and dynamics of the atmosphere, starting from some initial state and moving forwards in time. Also known as General Circulation Models (GCMs), their run times are longer, but allow for simulation of new scenarios and can capture smaller scale structures.

Sources of errors in GCM forecasts, along with the approximate ratios and timescales they appear on are demonstrated in Figure 1. The initial conditions of a GCM can dominate the early errors within a forecast as the model moves from this background towards a more steady state reflective of the later inputs. Careful selection of these initial conditions, such that they more accurately describe the true state of the atmosphere, can drastically reduce these errors. Alternatively the model can be spun-up by modelling a number of days prior to the forecast using the recently observed solar indices. Long-lived molecules which alter the radiative balance of the thermosphere, such as carbon dioxide, can have a prolonged effect if incorrect in the initial conditions. The overall uncertainty will reduce as the initial conditions move closer to the true state, and so in the short-term (hours to a week) the majority of the error can be attributed to the model itself.

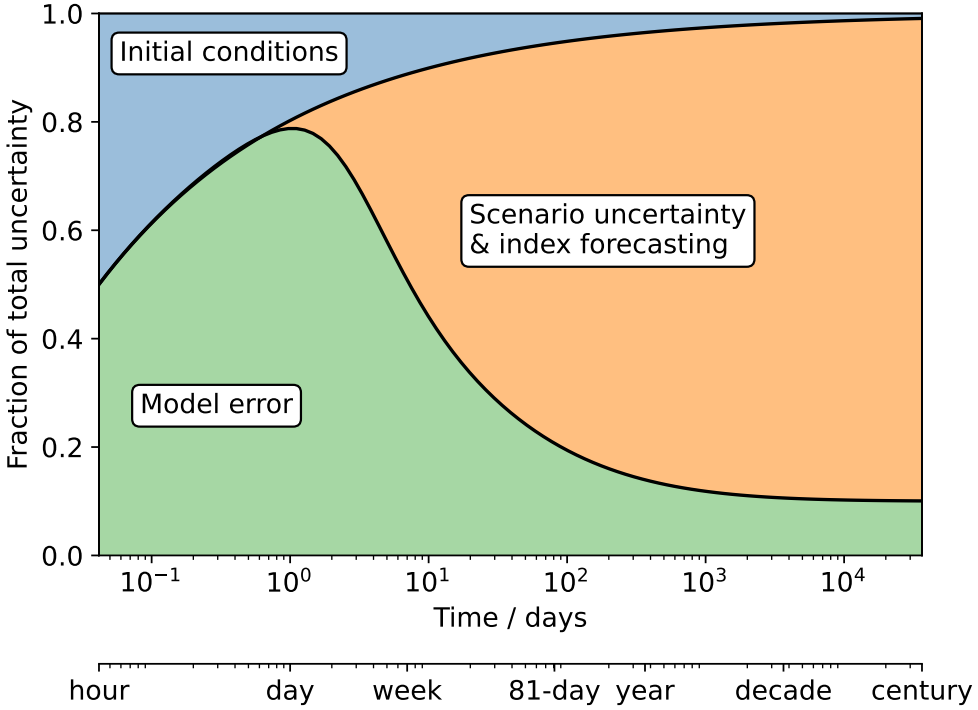

Fig. 1: The estimated sources of uncertainty in general circulation modelling over time. Values are meant for demonstration purposes, as exact values vary across models, variables and methodologies.

In the longer-term, the uncertainty within the driving variables of the model become the dominant source of error. The F10.7 cm solar ratio flux and Kp geomagnetic disturbance indices are common proxies for solar activity. Forecasts of F10.7 on the time scale of a week perform well due to the slow variation in the proxy. However, Kp can vary rapidly

over this timescale due to the difficulty of predicting events such as Coronal Mass Ejections (CMEs). The Sun rotates every 27 days, so satellites viewing the far-side of the Sun can provide advance warning of active regions and improve Kp forecasts. As solar activity indices are used in empirical models, the largest source of uncertainty shifts from the model itself to the forecasts of these indices. The 81-day averaged F10.7 is used to reflect the "background" residual energy within the thermosphere in empirical models, and the full extreme ultraviolet spectrum within numerical models. This average requires forecasting 40 days into the future or incorrectly using a window looking at 81-days prior to the current time step [5]. Data gaps in these solar indices can also affect model error, as demonstrated recently with an outage on 18 March 2022 in F10.7 provision caused by a cyberattack, and lasting for over a month in length [6].

Even if the model was perfect, the choice of scenario becomes the major source of uncertainty when looking on the order of years to decades. The approximately 11-year solar cycle sees an order of magnitude change in thermospheric density. But forecasting the amplitude and length of the next, or even current, solar cycle is still an active area of research. There were over 30 forecasts of the current solar cycle 25, with a mean and standard deviation across these of the sunspot number being 136.2 ± 41.6, and ranging from 50 to 233 [7, 8, 9]. Further, these forecasts change as more information about the current cycle is available, with the forecast of 233 being revised to 184 ± 17 sunspots [10]. There is also the possibility of a period of sustained low solar activity, as happened within the Maunder minimum.

Carbon dioxide is not only in the troposphere, with similar concentrations present in the atmosphere up to the homopause at around 90 km, as shown in Figure 2. The concentration then drops rapidly as the altitude increases in the mesosphere and lower part ($<$ 150 km) of the thermosphere (MLT). Ground-level CO_2 emissions affect the CO_2 concentration throughout the atmosphere, with higher concentrations in the MLT resulting in cooling of the upper atmosphere and thermospheric contraction. This in turn leads to a long-term trend of neutral density reduction within the upper atmosphere [11]. This is as the thermosphere exchanges energy by molecular diffusion with the MLT, which acts as a heat sink, radiating energy away via CO_2 and nitric oxide (NO). The historical neutral density decrease ranges from -2 to -5% per decade at 400 km, with the value depending upon solar activity levels. However, this rate of decrease is tied to the rate of CO_2 emissions and so may change in the future, as will be addressed in Section 3.

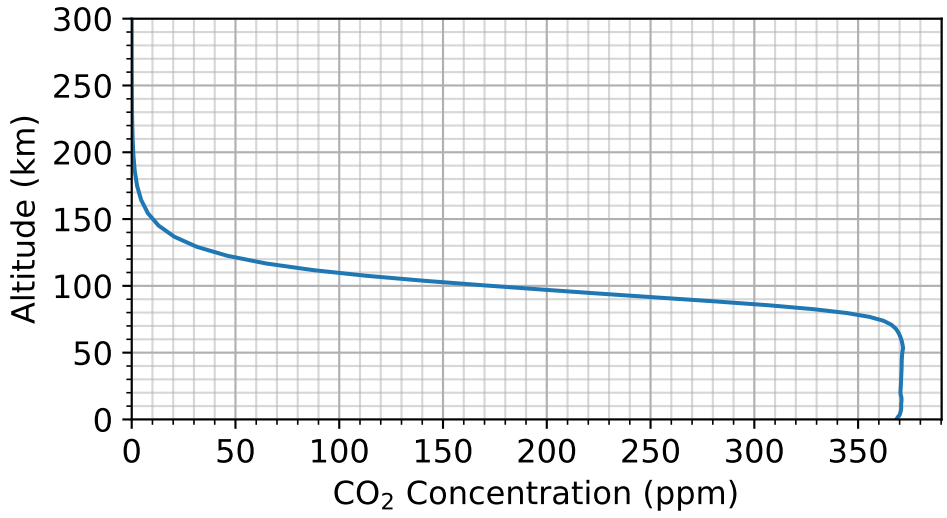

Fig. 2: Altitude profile of carbon dioxide concentration for the year 2000, using global average of the default WACCM-X initial files.

There are other, much smaller long-term trends. For example, the movement of the Earth's magnetic field is predicted to cause a 1-2% increase in global mean thermospheric neutral density between 2015 and 2065 [12, 13]. But a potentially substantial long-term trend comes about from the increased use of space, with a larger number of satellites re-entering the Earth's atmosphere and depositing aluminium within the MLT. This changes the albedo and radiative properties of the region [14]. However, research into this is at an early stage, with the amount of deposited aluminium being uncertain, and the chemistry required to model the impacts only recently being added to specific GCMs [15].

2. SHORT-TERM FORECASTING (WEATHER)

Accurate orbital propagation over the timescale of hours to days is becoming increasingly important within LEO. As the number of objects in the region increases, so does the number of potential conjunctions. Reducing orbital uncertainty, particularly via better characterised neutral densities in LEO, will extend the window of time during which the information is actionable for decision-makers, reducing the frequency of unnecessary manoeuvres. Satellites in temporary holding, or sustained, low altitude orbits are more susceptible to sudden increases in neutral density. This was demonstrated during the moderate-Kp "Starlink storm" in February 2022, which resulted in the reentry of 38 out of 49 recently launched Starlink satellites [16]. Improved forecasts and use of updated thermospheric density models can help mitigate these impacts.

Data assimilation provides a solution to the short-term forecast problem, debiasing numerical models through the use of recent observations, providing quantification of the uncertainty within the current atmospheric system, and adapting to circumstances not captured within the climatology of empirical models. The application of data assimilation for neutral density forecasting within the UK is discussed in Section 2.1.

2.1 Data Assimilation: AENeAS at the UK MOSWOC

SWIMMR (Space Weather Instrumentation, Measurement, Modelling and Risk) is a £20 million, four-year programme to improve the UK's capability for space weather monitoring and prediction. A subset of this is SWIMMR-T, looking at thermospheric density forecasting on short and long timescales. For short-term forecasting up to 48 hours, the Advanced Ensemble electron density Assimilation System (AENeAS) is currently being made operational at the UK's Met Office Space Weather Operations Centre (MOSWOC), with an aim to provide neutral densities to end users by Q3 2024.

AENeAS is a 4D physics-based data assimilation model of the ionosphere-thermosphere system [17]. It uses the Thermosphere Ionosphere Electrodynamics General Circulation Model (TIE-GCM) as the background numerical model [18], allowing physics-based nowcasting and forecasting from an observation-constrained hindcast. Assimilation is performed via a local ensemble transform Kalman filter (LETKF). For a standard Kalman Filter, starting from a background state vector, $\boldsymbol{x}_b$, and its associated error covariance matrix $\boldsymbol{B}$, an updated state vector $\boldsymbol{x}_a$ (a.k.a the analysis), and its associated error covariance matrix, $\boldsymbol{A}$, are obtained by

$$\boldsymbol{A} = (\boldsymbol{I} - \boldsymbol{K}\boldsymbol{H})\boldsymbol{B} \tag{1}$$

$$\boldsymbol{x}_a = \boldsymbol{x}_b + \boldsymbol{K}(\boldsymbol{y}_o - \boldsymbol{H}\boldsymbol{x}_b) \tag{2}$$

where

$$\boldsymbol{K} = \boldsymbol{B}\boldsymbol{H}^T(\boldsymbol{H}\boldsymbol{B}\boldsymbol{H}^T + \boldsymbol{O})^{-1} \tag{3}$$

and $\boldsymbol{I}$ is the identity matrix, $\boldsymbol{K}$ is the Kalman gain matrix, $\boldsymbol{H}$ is the observation operator, $\boldsymbol{y}_o$ is the vector of observations, and $\boldsymbol{O}$ is the observation error covariance matrix.

For the LETKF, the single background state vector in the above, standard Kalman filter, namely $\boldsymbol{x}_b$, is replaced by a set of n background ensemble members, $\boldsymbol{x}_{b(i)}$ where i takes values between 1 and n. The mean of these ensemble members, $\bar{\boldsymbol{x}}_b$, gives the best estimate of the true background state. A matrix of background perturbations, $\boldsymbol{X}_b$, can be constructed by setting the ith column to be equal to $\boldsymbol{x}_{b(i)} - \bar{\boldsymbol{x}}_b$. The background error covariance is then estimated by

$$\boldsymbol{B} = (n-1)^{-1}\boldsymbol{X}_b(\boldsymbol{X}_b)^T \tag{4}$$

which when substituted into Equation 3 gives the Kalman gain for the LETKF, namely

$$\boldsymbol{K} = (n-1)^{-1}\boldsymbol{X}_b(\boldsymbol{H}\boldsymbol{X}_b)^T[(n-1)^{-1}\boldsymbol{H}\boldsymbol{X}_b(\boldsymbol{H}\boldsymbol{X}_b)^T + \boldsymbol{O}]^{-1} \tag{5}$$

A full derivation and explanation of the LETKF is given in [17] and references within.

Previously, AENeAS used solely ionospheric measurements to constrain the thermosphere. In particular, electron density true height profiles from ionosondes, and total electron content (TEC) measurements from global navigation

satellite system (GNSS) receivers. As the state vector contains thermospheric neutral densities and electron densities, any electron density measurements self-consistently update the neutral densities too (along with all other variables in the state vector, such as neutral winds). This methodology has been shown to reduce the bias between the background model and accelerometer-derived measurements of neutral density by the Challenging Minisatellite Payload (CHAMP) satellite [2].

Before being made fully operational, observations of neutral density will be included within the assimilation. This is being done via Orbital Mean-elements Messages (OMMs), whose information was previously distributed via Two-Line Element sets (TLEs). From a pair of OMMs, the average density along the trajectory can be derived by considering the energy dissipation rate (EDR) required to explain the reduction in semi-major axis between the OMMs (a.k.a. the increase in the mean of mean motion) [19].

Outliers and manoeuvres within the OMM database can introduce nonphysical and inaccurate derived-densities into the assimilation process. To address this, OMMs for each object are preprocessed prior to density derivation using the Tracking Real-time Unusual Satellite Trajectories (TRUST) algorithm, with an example shown in Figure 3. This is based upon the Density-Based Spatial Clustering of Applications with Noise (DBSCAN) clustering algorithm which groups data with nearby neighbours. The default DBSCAN uses a circle of fixed radius of each data point, with any other data points falling inside that circle being denoted a neighbour. Once a user-defined number of neighbours are found, a cluster is formed, and all neighbours of points within the cluster are recursively labelled as being in the cluster themselves. TRUST builds upon this by, for each individual object, using a box in four-dimensional space covering semi-major axis, eccentricity, inclination and epoch. The size of the box varies to the expected difference in each parameter for that object. For example, the distance between neighbouring OMMs in semi-major axis decreases with increasing altitude, as smaller changes in semi-major axis are expected due to the lower neutral density and atmospheric drag at these altitudes.

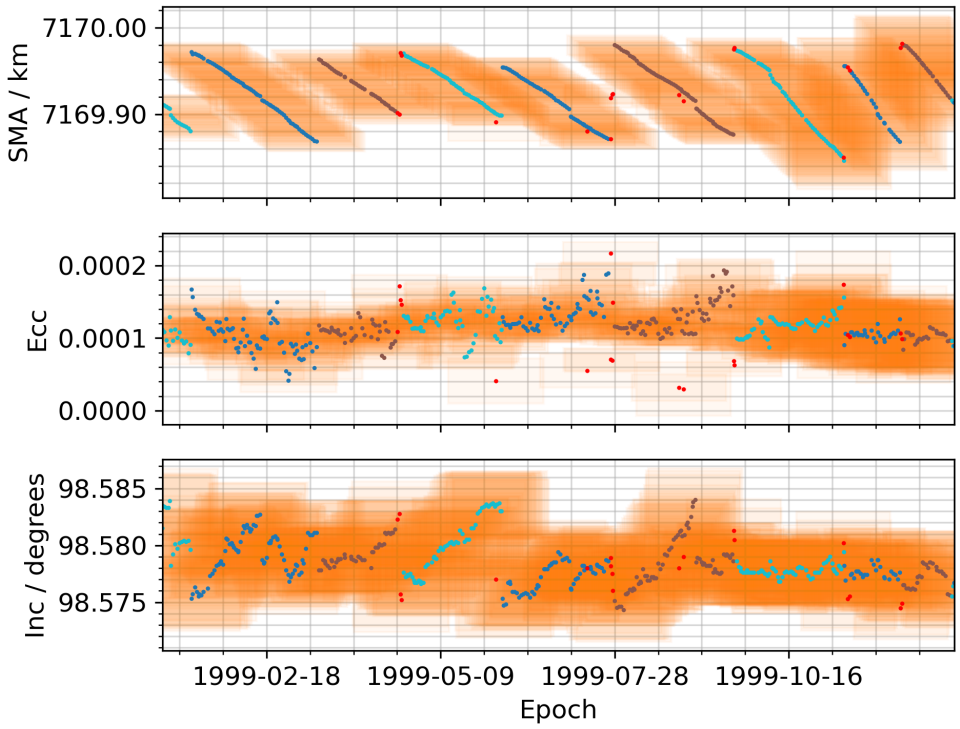

Fig. 3: An example of the TRUST algorithm applied to RADARSAT (NORAD ID 23710) over the year 1999. Subfigures show semi-major axis (SMA), eccentricity (Ecc) and Inclination (Inc) over time. Light blue, dark blue and brown points indicate unique clusters, alternating between the colours over time. Red points indicate outliers in the 4D space. Orange boxes are drawn around each point to demonstrate the ”neighbourhood” region.

Operationally including OMM-derived densities within AENeAS is challenging due to the computational cost of running an ensemble of 32 or more instances of TIE-GCM on the timescales needed to assimilate the approximately 24-hour averaged OMM-derived density observations. The current plan is to use an intermediary model to perform four-dimensional variational (4D-Var) assimilation of the OMM-derived densities with a simple background model [20]. This will allow the assimilation of neutral densities to take place over a larger timescale with significantly less computational expense compared to AENeAS. The intermediary model can then provide the assimilated neutral densities at a finer time step and shorter timescale to AENeAS, while still including the information prior to the AENeAS analysis window.

The choice of a simple background model (such as an exponential model with day-night variation and simple F10.7 effects [21]) is made as 4D-Var requires a tangent linear model, effectively a full differential version of the model. This is a substantial task even for basic empirical models. With enough observations, a large initial guess error should be overcome within the assimilation while still providing a method to move the atmospheric state forward in time. More complex neutral density models and their tangent linear versions can replace the simple one in future work.

The vertical coordinate of GCMs are pressure levels instead of altitude. TIE-GCM's, and therefore AENeAS's, upper boundary altitude therefore varies in latitude, longitude and time as the energy input to the system changes. In general, it varies between around 400 and 700 km, above which the atmosphere can no longer be modelled as a fluid and the underlying Navier-Stokes equations and assumptions breakdown. Observations above the maximum model altitude cannot be assimilated, and forecasts are limited in height so do not capture altitudes of interest within LEO. In AENeAS, this issue was already addressed for ionospheric observations by increasing the electron density model height with the use of NeQuick, an empirical model of electron concentrations [22]. To address the issue for neutral density observations, the upper boundary of TIE-GCM was increased in altitude. Previous methods have achieved this by increasing the number of pressure levels and assuming similar conditions to the original top-of-model [23]. A significant number of levels have to be added to ensure capturing all of LEO (up to 2000 km) in all solar activity conditions, substantially adding to run-time. Instead, the number densities of neutral constituents are extrapolated to higher altitudes using a Bates-Walker profile fit to the modelled region [24, 25, 26]. This profile can be summarized by

$$n(i|z) = n(i|\infty) exp\left[-\frac{m_i g_{ref}}{kT_\infty} \frac{(z - z_\infty)(R + z_{ref})}{R + z} \right] \tag{6}$$

where $n(i|z)$ is the number density of constituent i at altitude z, m_i is the mass of the constituent, g_{ref} is the gravity at the reference altitude z_{ref} (taken as a few levels below the top level of TIE-GCM), k is the Boltzmann constant and R is the Earth's radius. While T_∞ is the exospheric temperature, it is not an output of TIE-GCM, so a value is taken a level below the top of model. z_∞ is the altitude at which the exospheric temperature is taken from TIE-GCM. Bates-Walker profiles are the backbone of empirical models such as MSIS-86 [26]. The majority of MSIS models focus on calculating the number density at a reference altitude of 120 km at a given location and solar indices, and the Bates-Walker profile then extrapolates that value to higher altitudes. Instead here the extrapolation takes place from a higher altitude, maintaining the variation in the thermosphere which has been numerically modelled by TIE-GCM, as shown in Figure 4. The number density can then be modelled at any given altitude, ensuring all-LEO coverage. The constituent number densities can be converted to a total neutral mass density. This allows all LEO observations to be assimilated into AENeAS along with the ability to provide forecasts for these higher altitudes.

One major obstacle still to be solved is the handling of ballistic coefficients within the derivation of neutral densities from OMMs. There are two potential paths, or a combination of them. The first is to focus on a few well-known objects in a similar way to the High accuracy satellite drag model's (HASDM) choice of around 40 objects, except with OMMs in place of direct observations [27]. If this proves too sparse a dataset, and assuming the unlikely scenario of no ionospheric measurements, AENeAS would relax to the background model. However, the LETKF assimilation method discussed earlier can account for errors within the assimilation process, by trusting observations with larger errors less so as to have a smaller impact on the analysis. So the second option is to use as many pairs of OMMs for as many objects as possible, and attempt to characterise the uncertainty in ballistic coefficients within the observation error covariance matrix. For known objects (i.e. most satellites), these errors could be derived from the spread of their potential cross-sectional areas. Otherwise, for uncharacterised objects such as debris, the BSTAR parameter within the OMMs / TLEs may need to be relied upon, despite its poor definition.

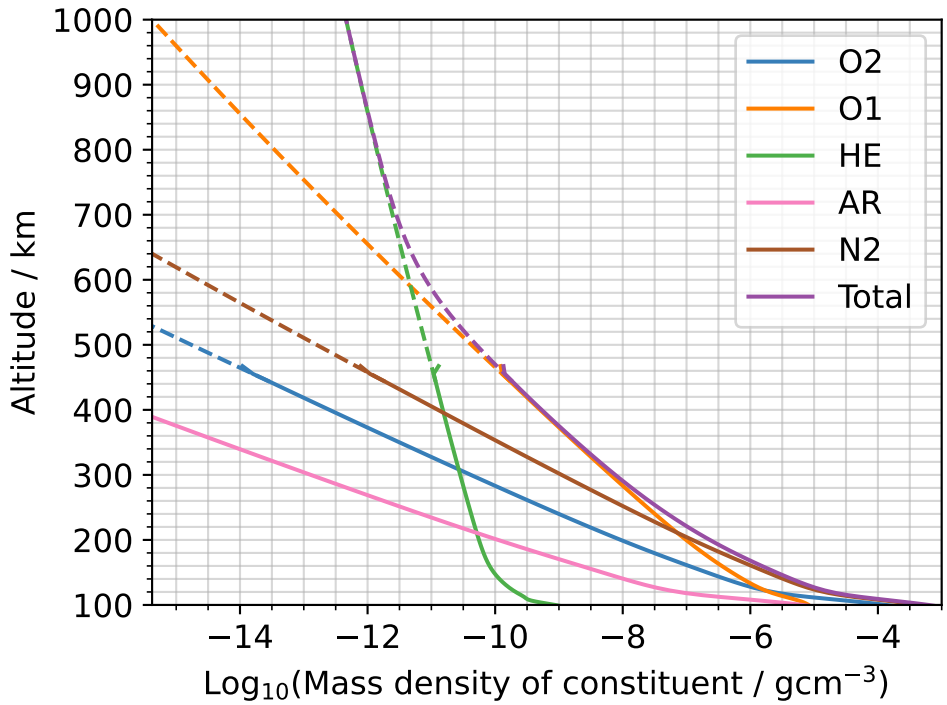

Fig. 4: An example of the extrapolation performed on TIE-GCM (and hence AENeAS) output at a given latitude, longitude and time, with the resulting total neutral density. Output from TIE-GCM is denoted by solid lines, while the extrapolation is dashed. TIE-GCM is known to have false values in the top-most layer (upper boundary), so extrapolation begins below this.

3. LONG-TERM FORECASTING (CLIMATE)

Long-term forecasts of exact neutral densities on the order of months to decades have huge uncertainties due to the reasons discussed in the introduction. This makes forecasts on this scale unfeasible for exact orbital propagation. However, scenarios and trends can still provide useful information, in a similar way to the impacts of El Niño or climate change on the future climatology within the troposphere. An example of this for the thermosphere is the long term trend of decreasing neutral densities due to carbon dioxide emissions, meaning empirical models based on decades-old data will be biased towards larger neutral densities. In turn, predictions of orbital lifetimes to match the 25, or 5, year rule for reentry could be significantly overshot if using these older density models, even with a perfect solar cycle prediction.

As discussed in Section 1, prediction of the amplitude and length of solar cycles is still an active area of research. Forecasts of the amplitude for the current solar cycle 25 varied dramatically between 50 and 233 sunspots. While noted, they are outside the scope of the work the authors have performed in this paper.

Instead, focus turns to the long-term, future impact of carbon dioxide upon the thermosphere, namely the trend of reducing densities. To simulate this, the thermosphere was modelled under increasing carbon dioxide concentrations using the Whole Atmosphere Community Climate Model with thermosphere and ionosphere extension (WACCM-X). The Intergovernmental Panel on Climate Change (IPCC) produced four Representative Concentration Pathways (RCPs), acting as potential scenarios meant to summarise the range of predictions in the literature up to that point [28]. These are RCP2.6, RCP4.5, RCP6.0, RCP8.5, with the number referring to the radiative forcing in W/m^2 in the year 2100. The CO_2 pathways are shown in Figure 5. These have been updated into the Shared Socioeconomic Pathways (SSPs) which include narratives defining the socioeconmic circumstances leading to each pathways, although the carbon dioxide profiles are similar to the RCPs [29].

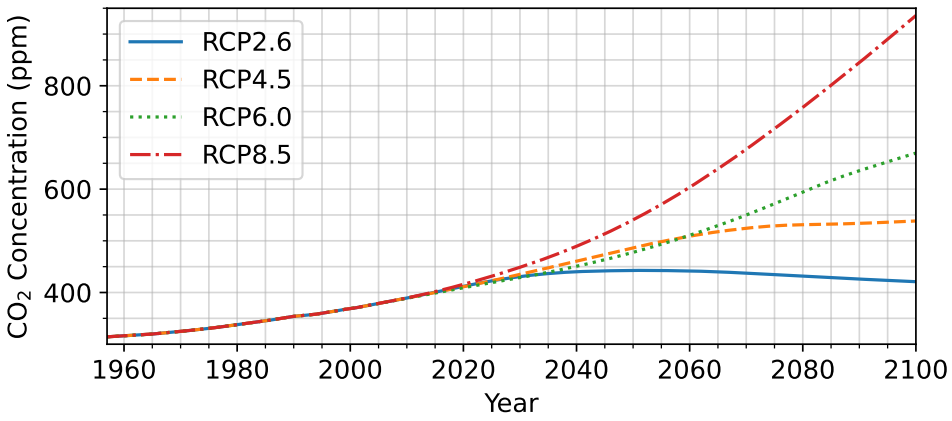

Fig. 5: Ground-level carbon dioxide concentrations through the space age, and future carbon dioxide scenarios of the Representative Concentration Pathways (RCPs) from the IPCC's fifth assessment report [28].

Ground-level CO_2 concentrations were taken from RCP8.5 in 10-year intervals from 2005 to 2095 inclusive, with these values later being mapped to the other RCPs. CO_2 concentrations are named by their ground-level value to allow direct comparison to wider climate change literature. The altitude profile of CO_2 (shown in Figure 2) was scaled to reflect the higher concentrations which would be observed throughout the atmosphere. WACCM-X was then run for a year prior to using output to allow minor constituents to reach a steady-state.

Studies of the historic period have shown the trend depends on solar activity, with the ratio of CO_2 to NO changing due to higher rates of dissociation under high solar activity, and in turn changing the radiative balance of the MLT region. To account for this, WACCM-X was run at a low (70 sfu) and high (200 sfu) F10.7 value for all modelled CO_2 values, and at 100, 135 and 170 sfu for a fixed CO_2 value of 639 ppm. The parameter space was limited to this range of values as global-mean annual-means are used to remove seasonal variations, and each year of WACCM-X simulation took 4 days to complete. Results are shown in Figure 6. The Paris Agreement corresponds to a CO_2 concentration of 480 ppm, which at 400 km relates to a neutral density reduction since the year 2000 of 15% under high solar activity, and 32% under low solar activity.

The F10.7 relationship (shape of curve) of Figure 6c is assumed to be similar at other CO_2 values. The curve can then be scaled so that the density reduction at F10.7 at 70 and 200 sfu matches those of Figures 6a and 6b for a given CO_2 value. This allows the neutral density reduction at any given CO_2 and F10.7 value to be found. By using the future carbon dioxide concentrations of the RCPs, shown in Figure 5, and by assuming solar cycle 24 repeats into the future, the future neutral density relative to the year 2000 can be given for four scenarios (named after the RCPs), as shown in Figure 7.

To investigate the impact these density reductions would have on the debris environment, they were used within the Binned Representative Atmospheric Decay (BRAD) debris model [11]. BRAD bins objects by semi-major axis, eccentricity, inclination, and mass. These bins covered the LEO orbits most affected by drag, namely circular orbits up to 1200 km and eccentric orbits up to 440 x 1957 km. Orbital propagation is performed on a representative object at the centre of each bin, shifting a virtual bin around it, and the overlap with the other bins determining how many objects have moved from the virtual bin to each of the other bins. Collisions are handled by calculating the chance of an object in each of two bins colliding, multiplying by the number of objects in each bin, and testing against a Poisson distribution [30]. If the check passes, the number and size of fragments are calculated by the NASA Standard Breakup Model [31]. These are then scattered across bins in semi-major axis and eccentricity, with the number of fragments reducing as the bins get further away. More details on BRAD are given in [11].

NRLMSISE-00 is used as the background model within BRAD, and assumed to give a true representation for the year 2000 [4]. A control scenario of BRAD is performed from the year 2000 to 2100 as a Monte Carlo of 32 runs, repeating solar cycle 24 and with launches repeating the years 2005-2013 (purposefully prior to megaconstellation launch traffic). The same methodology and inputs are than used with BRAD under the RCP scenarios of Figure 5.

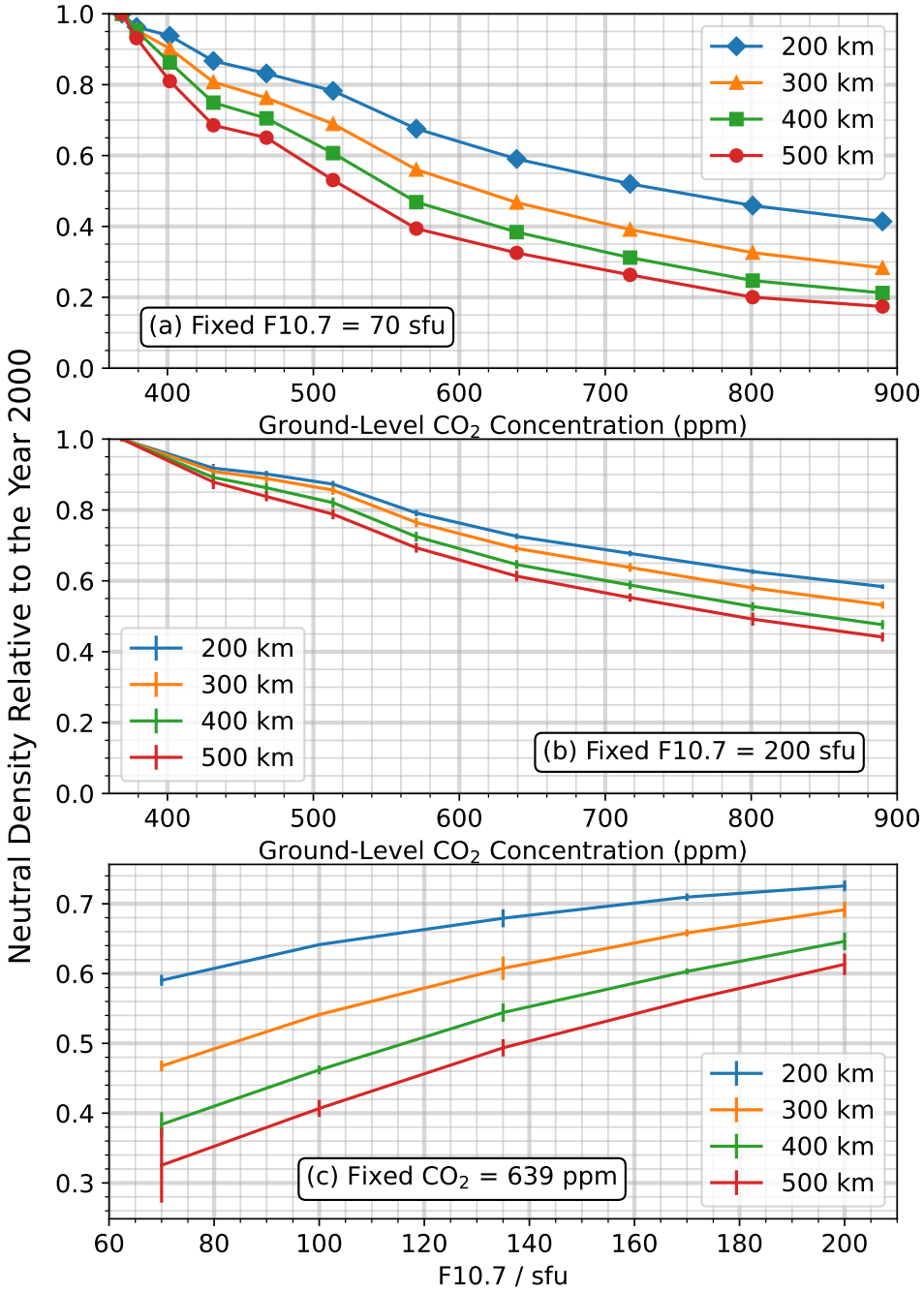

Fig. 6: Future density reductions modelled with WACCM-X. (a) is the low solar activity (F10.7 = 70 sfu) study, varying carbon dioxide concentration. (b) is the high solar activity (F10.7 = 200 sfu) study, varying carbon dioxide concentration. (c) is the varying solar activity, using a fixed CO_2 of 639 ppm, and with a zoomed-in y axis compared to the other 2 subfigures.

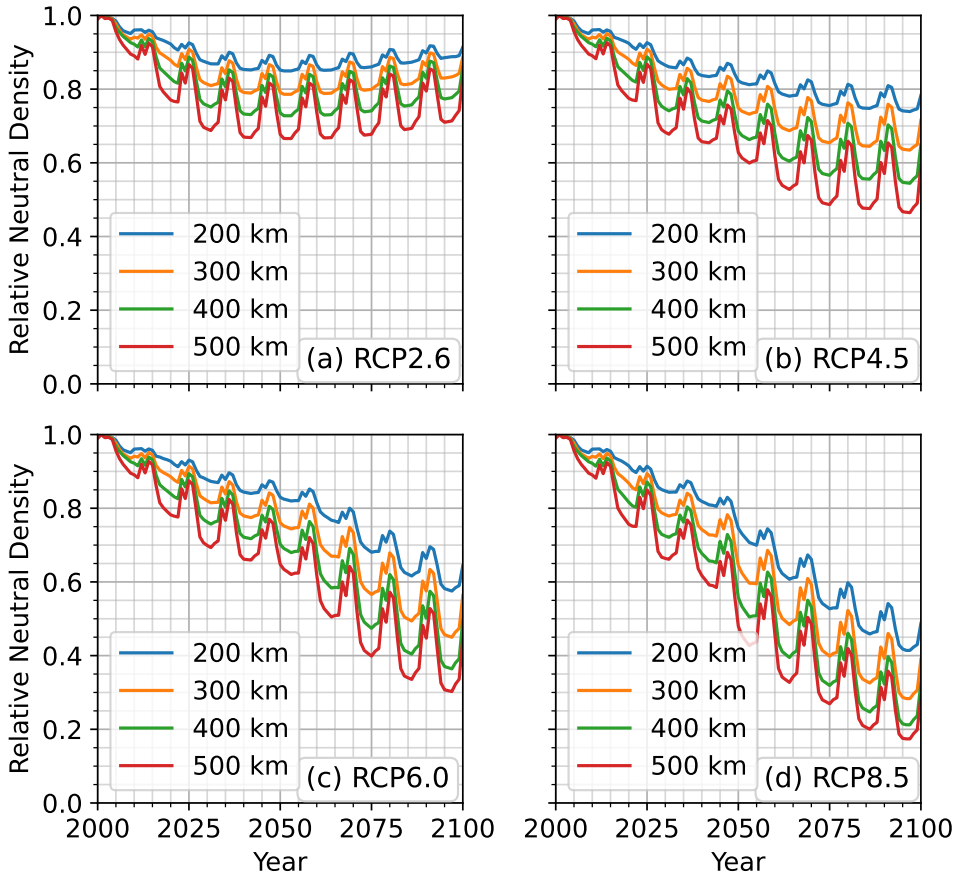

Fig. 7: Future density reduction scenarios with solar cycle 24 repeating for each of the RCPs. Modelled using WACCM-X and converting the global-mean annual-mean densities of the low, high and varying solar activity runs into a lookup table.

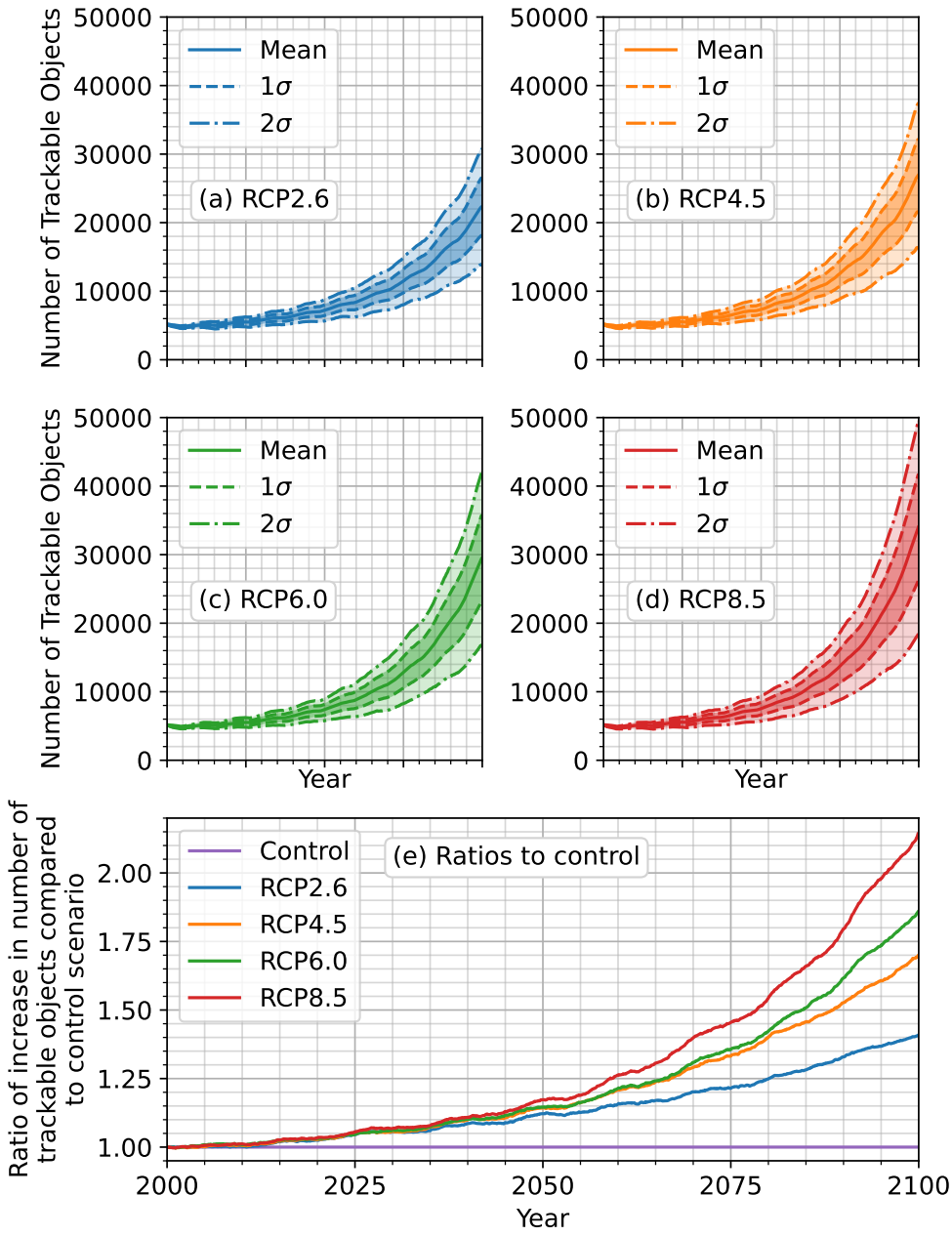

Fig. 8: The number of trackable objects in LEO modelled by BRAD over the period 2000 to 2100 under the reduced neutral densities of the RCP scenarios. Launches repeated 2005-2013 (pre-megaconstellation traffic) and solar cycle 24 repeats. Subfigure e gives the ratios of the above figures against the control scenario (no density reductions applied to NRLMSISE-00).

The future densities are obtained by multiplying the density from NRLMSISE-00 by the scale factors given in Figure 7. The increase in the number of objects in these scenarios is shown in Figure 8a-d, and as a ratio against the control scenario in Figure 8e. As neutral densities reduce due to increasing carbon dioxide concentrations, the number of objects in LEO will increase at a faster rate. This is due to objects having longer orbital lifetimes, but also this increasing the probability of them experiencing a collision during their lifetime.

The RCP2.6 scenario is of particular interest. It is known as the “peak-and-decline” scenario due to carbon dioxide

concentrations reaching their maximum in 2050 and falling. The neutral atmospheric density in LEO follows a similar trajectory, with the largest reduction (i.e. smallest densities) in 2050, and then density increasing post-2050 (see Figure 7). However, from Figures 8a and 8e, the number of objects, and the rate of increase, continues to rise post-2050. The recovering neutral densities cannot remove objects at a faster rate than the fragmentations caused by the higher number of objects and collisions in the pre-2050 environment.

4. CONCLUSIONS

Forecasting future neutral densities raises different challenges depending upon the timescale. On the short timescale (hours to days), data assimilation can address the larger errors caused by model bias by incorporating observations. AENeAS is a data assimilation model being made operational at the UK MOSWOC, and will provide neutral densities for spacecraft operators. While currently using ionospheric measurements to constrain the thermosphere, thermospheric measurements are being added via derived densities from OMMs (previously TLEs). This will be done by an intermediary model using 4D-Var to best make use of the 24-hour average densities obtained from OMMs.

On the longer-term (years to decades), the choice of scenario becomes important. Increasing carbon dioxide concentrations in the MLT region lead to decreasing neutral densities within the thermosphere, with this leading to reduced atmospheric drag on satellites and longer orbital lifetimes. This has been modelled with WACCM-X for four carbon dioxide pathways scenarios, and neutral density reductions presented. Under the best-case scenario, RCP2.6, neutral densities will be between 15% and 32% under high and low solar activity respectively (with this change applied on top of the usual order-of-magnitude change due to the solar cycle).

To investigate the impact on the debris environment, the BRAD debris model was used to model the LEO environment under each of the RCP scenarios, along with a control (no density reduction). It is shown that the decreased neutral densities increase the number of objects in LEO, both through increased orbital lifetimes and the increased probability of collision during a lifetime. Under the best-case scenario, RCP2.6, there are 40% more objects in LEO by 2100 compared to the control scenarios, with this reaching more than 210% in the worst-case RCP8.5 scenario. This is a significant source of future orbital debris which has not been included in most debris models covering LEO.

5. REFERENCES

[1] O. Montenbruck, E. Gill, and F. H. Lutze. Satellite orbits: models, methods, and applications. *Appl. Mech. Rev.*, 55(2):B27–B28, 2002.

[2] S. Bruinsma, T. D. de Wit, T. Fuller-Rowell, K. Garcia-Sage, P. Mehta, F. Schiemenz, Y. Y. Shprits, R. Vasile, J. Yue, and S. Elvidge. Thermosphere and satellite drag. *Advances in Space Research*, 2023.

[3] J. T. Emmert. Thermospheric mass density: A review. *Advances in Space Research*, 56(5):773–824, 2015.

[4] J. M. Picone, A. E. Hedin, D. P. Drob, and A. C. Aikin. NRLMSISE-00 empirical model of the atmosphere: Statistical comparisons and scientific issues. *Journal of Geophysical Research: Space Physics*, 107(A12):SIA–15, 2002.

[5] E. Donegan-Lawley, S. Elvidge, L. Nugent, A. Wood, and D. Themens. Two different (and commonly used) methods of calculating the 81-day average value of the F10.7 cm solar radio flux: Impacts of global models. In *Beacon Satellite Symposium 2022*, 2022.

[6] S. Elvidge, D. R. Themens, M. K. Brown, and E. Donegan-Lawley. What to do when the F10.7 goes out? *Space Weather*, 21(4):e2022SW003392, 2023.

[7] D. Nandy. Progress in solar cycle predictions: Sunspot cycles 24-25 in perspective. *Solar Physics*, 296(3):54, 2021.

[8] I. N. Kitiashvili. Application of synoptic magnetograms to global solar activity forecast. *The Astrophysical Journal*, 890(1):36, 2020.

[9] S. W. McIntosh, S. Chapman, R. J. Leamon, R. Egeland, and N. W. Watkins. Overlapping magnetic activity cycles and the sunspot number: forecasting sunspot cycle 25 amplitude. *Solar Physics*, 295(12):1–14, 2020.

[10] S. W. McIntosh, R. J. Leamon, and R. Egeland. Deciphering solar magnetic activity: The (solar) Hale cycle terminator of 2021. *Frontiers in Astronomy and Space Sciences*, 10:16, 2023.

[11] M. K. Brown. *Climate Change in Space: The Impact on Space Debris*. PhD thesis, University of Southampton, 2023.

[12] I. Cnossen and A. Maute. Simulated trends in ionosphere-thermosphere climate due to predicted main magnetic field changes from 2015 to 2065. *Journal of Geophysical Research: Space Physics*, 125(3):e2019JA027738, 2020.

[13] I. Cnossen. A realistic projection of climate change in the upper atmosphere into the 21st century. *Geophysical Research Letters*, 49(19):e2022GL100693, 2022.

[14] A. C. Boley and M. Byers. Satellite mega-constellations create risks in low earth orbit, the atmosphere and on Earth. *Scientific Reports*, 11(1):10642, 2021.

[15] J. M. C. Plane, S. M. Daly, W. Feng, M. Gerding, and J. C. Gómez Martín. Meteor-ablated aluminum in the mesosphere-lower thermosphere. *Journal of Geophysical Research: Space Physics*, 126(2):e2020JA028792, 2021.

[16] T. E. Berger, M. Dominique, G. Lucas, M. Pilinski, V. Ray, R. Sewell, E. K. Sutton, J. P. Thayer, and E. Thiemann. The thermosphere is a drag: The 2022 Starlink incident and the threat of geomagnetic storms to low earth orbit space operations. *Space Weather*, 21(3):e2022SW003330, 2023.

[17] S. Elvidge and M. J. Angling. Using the local ensemble transform Kalman filter for upper atmospheric modelling. *Journal of Space Weather and Space Climate*, 9:A30, 2019.

[18] L. Qian, A. G. Burns, B. A. Emery, B. Foster, G. Lu, A. Maute, A. D. Richmond, R. G. Roble, S. C. Solomon, and W. Wang. The NCAR TIE-GCM: A community model of the coupled thermosphere/ionosphere system. *Modeling the ionosphere–thermosphere system*, pages 73–83, 2014.

[19] J. M. Picone, J. T. Emmert, and J. L. Lean. Thermospheric densities derived from spacecraft orbits: Accurate processing of two-line element sets. *Journal of Geophysical Research: Space Physics*, 110(A3), 2005.

[20] F. Bouttier and P. Courtier. Data assimilation concepts and methods March 1999. *Meteorological training course lecture series. ECMWF*, 718:59, 1999.

[21] G. E. Cook, D. G. King-Hele, and D. M. C. Walker. The contraction of satellite orbits under the influence of air drag. I. with spherically symmetrical atmosphere. *Proceedings of the Royal Society of London. Series A. Mathematical and Physical Sciences*, 257(1289):224–249, 1960.

[22] B. Nava, P. Coisson, and S. M. Radicella. A new version of the NeQuick ionosphere electron density model. *Journal of atmospheric and solar-terrestrial physics*, 70(15):1856–1862, 2008.

[23] Y. Cai, X. Yue, W. Wang, S. Zhang, H. Liu, D. Lin, H. Wu, J. Yue, S. L Bruinsma, F. Ding, et al. Altitude extension of the NCAR-TIEGCM (TIEGCM-X) and evaluation. *Space Weather*, 20(11):e2022SW003227, 2022.

[24] D. R. Bates. Some problems concerning the terrestrial atmosphere above about the 100 km level. *Proceedings of the Royal Society of London. Series A. Mathematical and Physical Sciences*, 253(1275):451–462, 1959.

[25] J. C. G. Walker. Analytic representation of upper atmosphere densities based on Jacchia's static diffusion models. *Journal of the Atmospheric Sciences*, 1965.

[26] A. E. Hedin. A revised thermospheric model based on mass spectrometer and incoherent scatter data: MSIS-83. *Journal of Geophysical Research: Space Physics*, 88(A12):10170–10188, 1983.

[27] M. F. Storz, B. R. Bowman, M. J. I. Branson, S. J. Casali, and W. K. Tobiska. High accuracy satellite drag model (HASDM). *Advances in Space Research*, 36(12):2497–2505, 2005.

[28] IPCC. *Climate Change 2014 Synthesis Report*. IPCC, 2014.

[29] J. S. Kikstra, Z. R. J. Nicholls, C. J. Smith, J. Lewis, R. D. Lamboll, E. Byers, M. Sandstad, M. Meinshausen, M. J. Gidden, J. Rogelj, et al. The IPCC sixth assessment report WGIII climate assessment of mitigation pathways: from emissions to global temperatures. *Geoscientific Model Development*, 15(24):9075–9109, 2022.

[30] R. Greenberg. Orbital interactions-a new geometrical formalism. *Astronomical Journal, vol. 87, Jan. 1982, p. 184-195.*, 87:184–195, 1982.

[31] N. L. Johnson, P. H. Krisko, J. C. Liou, and P. D. Anz-Meador. NASA's new breakup model of EVOLVE 4.0. *Advances in Space Research*, 28(9):1377–1384, 2001.